Modelling quantum optical processes, interference and correlations in novel microstructures

S.C. Skipsey[a], M. Babiker[a], M. Al-Amri[b] and G. Juzeliūnas[c]

[a] Department of Physics, University of York, Heslington, York YO10 5DD, England
[b] Department of Physics, King Khalid University, Abha, PO Box 9003, Saudi Arabia
[c] Vilnius University Research Institute of Theoretical Physics and Astronomy, A. Goštauto 12, 2600 Vilnius, Lithuania

ABSTRACT

The properties of localised dipole emitters in the form of a quantum dot or a colour centre embedded in a crystal environment can be drastically modified by a change in the composition, size and shape of the environment in which the emitter is embedded. Thanks to recent advances in material deposition techniques and lithography, as well as the advances in detection techniques and optical manipulation, experimental work is now capable of revealing a new range of physical phenomena when the typical dimensions are of the order of an optical dipole transition wavelength and below. These advances have arisen at a time of a heightened research effort devoted to the important goal of identifying a qubit and a suitable environment that forms the basis for a scalable hardware architecture for the practical realisation of quantum information processing. A physical system that we have recently put forward as a candidate for such a purpose involves localised emitters in the form of quantum dots or colour centres embedded in a nanocrystal. This suggestion became more persuasive following the success of experiments which, for the first time, were able to demonstrate quantum cryptography using a nitrogen vacancy in a diamond nanocrystal as a single-photon source. It has, however, been realised that a more versatile scenario could be achieved by making use of the interplay between dielectric cavity confinement and dipole orientation. Besides position dependence the main properties exhibit strong dipole orientational dependece suggesting that the system is a possible candidate as a qubit for a scalable hardware architecture for quantum information processing. Cavity confinement can control processes since it can lead to the enhancement and the complete suppression of the de-excitation process, with further control provided by the manipulation of the dipole orientation by optical means. This article is concerned with the modelling of quantum processes for quantum systems localised in artificially fabricated structures made of high conductivity metals and dielectric cavities. The essential features of cavity field confinement in this context are presented and the effects on de-excitation rates are assessed.

1. INTRODUCTION

Electromagnetic field confinement due to surfaces in material cavities of typical length scales comparable to an optical dipole transition wavelength involves a set of modes that are restricted in both spatial and spectral distributions relative to the case in the unbounded bulk. These restricted modes have important consequences for the properties of quantum systems that are localised at sub-wavelength distances from cavity surfaces. When the typical cavity dimensions are on the nanometre to micrometer scale, most of the familiar quantum phenomena are liable to change. For instance, spontaneous emission can be drastically reduced or enhanced and it can even be completely suppressed.[1] The quantum system in question can be any system capable of excitation and de-excitation, for example by optical means: neutral atoms, ions, molecules, quantum wells, quantum dots and quantum wires. A variety of effects are realisable, depending on the geometry and the material constituents forming the structure. Recent advances in material deposition techniques and lithography,[2] together with the advances in detection and optical manipulation of individual atoms and molecules,[3] are now capable of revealing a new range of physical phenomena when the typical length scales become comparable to or smaller than an optical dipole transition wavelength.

The simplest cavity effects occur when real space is divided into two half-spaces, one half-space is occupied by a perfect conductor, while the other half space is occupied by a dielectric or vacuum. A quantum system interacts with the electromagnetic fields that are confined by the metallic half-space. The next system in the

Nanomodeling II, edited by Akhlesh Lakhtakia, Sergey A. Maksimenko,
Proc. of SPIE Vol. 6328, 63280U, (2006) · 0277-786X/06/$15 · doi: 10.1117/12.679007

order of complexity is that of two parallel thick conductor slabs separated by a dielectric.[4] This system should, in principle, exhibit quantum charge states of a complicated nature than those arising for a single conductor. Such states have been shown to be akin to bonding and anti-bonding states similar to those of the hydrogen molecule ion. The theme of planar conductors forming a cavity can be generalised one step further to the case in which two conductors intersect at a general angle of intersection. For an acute angle of intersection, we have a wedge and the three dimensional analogue of the wedge is a corner, arising from the intersection of three conductors, the simplest of which is the case where the intersections form right angles. The interaction of an excited dipole emitter in the presence of conductors leads to a shift in the transition frequency and modifications of the rate of de-exciation[5].[6]

Other structures formed of planar conductors would be a waveguide with a rectangular cross-section and a quantum dot formed of six planar surfaces for which the confined fields are also well known and their influence on quantum systems localised within it are calculable in a straightforward manner[7].[8] Continuing along the perfect conductor theme, the next cases generalise the Cartesian geometry to cylindrical[9] or spherical[11] symmetry. An obvious case here is that involving a cylindrical structure with a diameter in the nanoscale, either forming a perfect quasi-one dimensional conductor (nanowire), or a cylindrical cavity in a conducting medium. Similarly a spherical quantum dot cavity in a conducting medium or a spherical conductor in vacuum are the natural generalisations of the nanostructures formed of planar surfaces.

Most of the cases discussed above deal with extreme confinement effects in cavity quantum electrodynamics where the perfect metal boundaries features prominently. More recently, the dielectric aspects of cavity quantum electrodynamics have been discussed in connection with quantum processes. In particular, the influence of a metallic film of nanometre thickness and finite conductivity deposited on a thick dielectric has been the subject of investigation[5].[6] One of the applications of such a multilayer structure is in atomic mirrors,[10] but its capability of supporting surface plasma modes leads to strong coupling to quantum systems in the near zone. The more general situation in which the two half spaces separated by the metallic film have different dielectric constants presents a much richer set of physical phenomena involving the participation of the full set of allowed modes, including evanescent and propagating modes as well as interface modes. This enables consideration of both the near-zone, which is dominated by the interface modes, and the far-zone, which is dominated by the remaining set of modes.

This paper is organised as follows. In section 2 we discuss the situation in the vicinity of a perfect mirror in the form of a perfect conductor half-space. This enables useful comparisons to be made with the results of the more complicated systems considered in the subsequent sections. In section 3 we describe the asymmetric dielectric structure comprising two semi-infinite dielectric layers separated by a thin metallic film of finite conductivity. We consider the coupling of the modes to a single dipole emitter localised on either side of the metallic film, which allows the variations of the de-excitation rate with the dielectric constants, the metallic areal electron density, the dipole orientation and the dipole position relative to the metallic film to be explored. Correlations between the dipole and its image are pointed out and we also discuss pair correlations involving cooperative effects exhibited by two real dipole emitters embedded in the structure and which can be located on the same side or on different sides of the metallic film. Sections 4 and 5 extend the planar surfaces theme in new directions, introducing a model of dipole relaxation in spaces with two (section 4) and three (section 5) mirror boundaries, forming an edge and a corner. It is shown that the behavior in these cases can be expressed in terms of the coupling of the dipole with all of its images in the mirrors, with the images themselves mutually non-interacting. The relevance of the work for quantum information processing is pointed out and discussed in the final section 6, along with comments and conclusions.

2. THE EFFECTS OF A PLANAR MIRROR

The simplest cavity effects arise in the situation where a perfect conductor occupies the half-space $z < 0$ and the second half-space $z > 0$ is a dielectric of dielectric constant ε. The perfect conductor is assumed to exclude all electromagnetic fields from its interior so that the interface at $z = 0$ is effectively a perfect mirror to all electromagnetic fields on the dielectric side. A dipole emitter localised in the dielectric can only interact with and via electromagnetic fields satisfying mirror boundary conditions. The de-exciatation rate for an excited

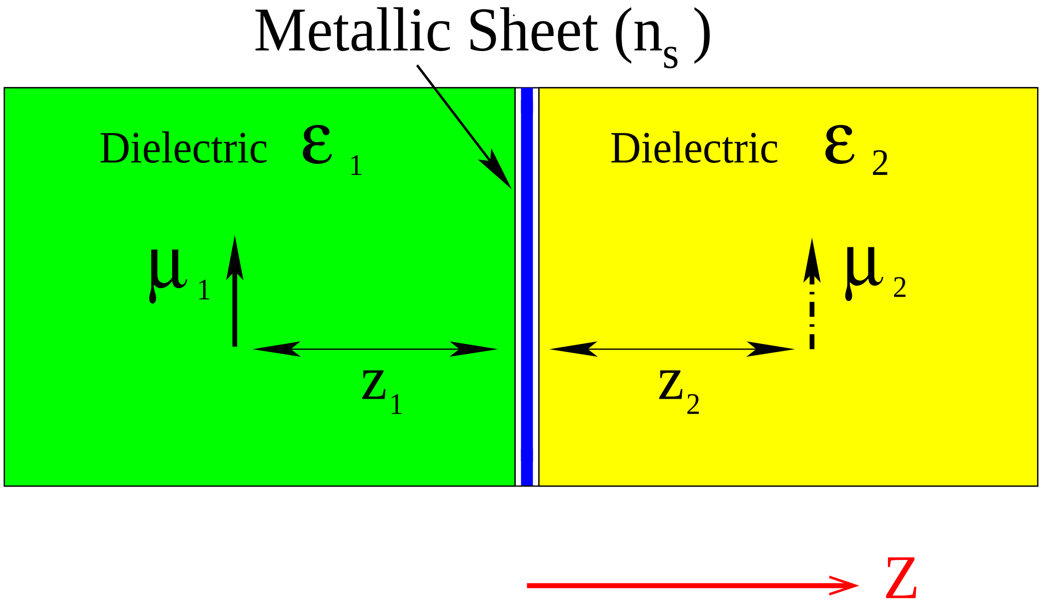

Figure 1: A schematic figure showing the asymmetric multilayer dielectric cavity, consisting of two dielectric half spaces of dielectric constants ε_1 and ε_2, separated by a thin metallic sheet with finite areal conductivity n_s. Dipole emitters on either side are shown as arrows.

emitter whose dipole moment vector is oriented in the direction $\hat{\boldsymbol{\mu}}$ is given by the Golden Rule:

$$\Gamma_{\hat{\boldsymbol{\mu}}}(\mathbf{R}) = \frac{2\pi}{\hbar^2 \varepsilon_0^2} \sum_Q \left| \langle e; \{0\} \left| -\boldsymbol{\mu}.\mathbf{D}(\mathbf{R}) \right| g; \{Q\} \rangle \right|^2 \delta(\omega(Q) - \omega_0) \tag{1}$$

where $\boldsymbol{\mu}$ is the transition diplole moment vector of the emitter, $|\{Q\}\rangle$ stands for a one-quantum state of the electromagnetic field satisfying the boundary conditions at the wedge surfaces, $\hbar\omega(Q)$ is the one-quantum energy and $|\{0\}\rangle$ stands for the electromagnetic vacuum field state. $\mathbf{D}$ is the quantised electric displacement field operator, evaluated at the position $\mathbf{R}$ of the emitter. The emitter is represnted here as a two-level system of excited state $|e\rangle$ and ground state $|g\rangle$ and a separation energy $\hbar\omega_0$, i.e. ω_0 is the dipole excitation frequency. Direct evaluations for a dipole emitter situated at a distance z from the surface yield the following results for a dipole parallel to the surface ($\Gamma_{\|}(z)$) and perpendicular to it ($\Gamma_{\perp}(z)$)

$$\Gamma_{\|}(z) = \Gamma_0 \left\{ 1 - \frac{3}{2} \left(\frac{\sin 2k_0 z}{2k_0 z} + \frac{\cos 2k_0 z}{(2k_0 z)^2} - \frac{\sin 2k_0 z}{(2k_0 z)^3} \right) \right\} \tag{2}$$

$$\Gamma_{\perp}(z) = \Gamma_0 \left\{ 1 - 3 \left(\frac{\cos 2k_0 z}{(2k_0 z)^2} - \frac{\sin 2k_0 z}{(2k_0 z)^3} \right) \right\} \tag{3}$$

where $k_0 = \omega_0/c$ and the rate is normalised in terms of the rate Γ_0 in an infinite dielectric given by $\Gamma_0 = 4\mu^2 k_0^3/(3\pi\varepsilon\hbar)$ where ε is the electric permittivity of the dielectric in which the emitter is embedded. This rate should be modified by a correction factor to account for the local field correction. The results can be interpreted as arising from a cooperative effect between the real dipole and its image in the conductor.[5]

3. ASYMMETRIC DIELECTRIC STRUCTURE

We now consider a planar dielectric cavity, as shown schematically in Fig.1, involving a finite conductivity metallic film occupying the plane $z = 0$, separating two dielctric half-spaces with ε_1 and ε_2 different dielectric constants. The thin metallic film is characterised by its finite electron density n_s and so has a finite conductivity σ at frequency ω, given by $\sigma = in_s e^2/\{m^*(\omega + i\gamma)\}$ where m^* and e are the electronic mass and charge in the metallic film and the small imaginary term $i\gamma$ in the denominator accounts for the plasma loss. The finite conductivity induces an in-plane electric current density $\mathbf{J}_{\|} = \sigma \boldsymbol{\mathcal{E}}_{\|}$ and this affects one of the electromagnetic boundary conditions involving the tangential magnetic field vector. We have $\hat{\mathbf{z}} \times \{\boldsymbol{\mathcal{H}}(z = 0_+) - \boldsymbol{\mathcal{H}}(z = 0_-)\} = \sigma \boldsymbol{\mathcal{E}}_{\|}(z = 0)$ where $0_\pm = \lim_{\eta \to 0}(\pm\eta)$. The magnetic field function follows from the electric field using Maxwell's equations.

In order to determine the mode functions we need the boundary condition, together with the continuity of the tangential component of the electric field at $z = 0$. There are three types of mode emerging from this procedure: (i) propagating modes, which have sinusoidal dependence in both regions of the structure; (ii) evanescent modes, which propagate in one region, but exponentially decay away from the interface in the other region and (iii) interface modes, which decay exponentially away from the interface in both regions of the structure. The de-excitation of quantum states occurs by emission into the three types of mode. Calculations are typically done by evaluating contributions from an individual type of mode and the result for a given situation is the sum of all contributions.

3.1. De-excitation of a single dipole emitter

Consider a single dipole emitter localised near the metallic film. Note that the novelty of this system stems partly from the fact that dipole emitters can be localised on either side of the film as shown in Fig 1. We evaluate the de-excitation rate analytically, but the results for a given set of parameters proceed using numerical methods. In particular, we can explore variations with the electron density n_s of the film and for varying emitter position, both in the near zone and in the far zone of the structure. The de-excitation rate is given by the Golden Rule, but now all the three types of mode described above participate in the de-excitation process. The details will not be presented here.[5] Figure 2 displays the variations of the emission rate with the electron density for an emitter fixed at the point $z = 50$nm. The parameters are such that $\varepsilon_2 = 1$, while ε_1 takes three diffferent values: $\varepsilon_1 = 1, 2$ and 3. The results of this figure show that the relaxation rate exhibits a minimum at low density which can be explained as due to screening arising from the propagating modes. As the density increases, the relaxation rate increases and exhibits a maximum at a density which is characteristic of that emitter position. The rate then decreases as the density increases further, diminishing to small values, consistent with the screening expected at much higher electron densities. The large density limit is formally identified as equivalent to the perfect conductor film limit where the metallic film completely screens electromagnetic fields sampled by dipole emitters located on either side of the film.

Figure 3 shows the variation with the emitter position of the relaxation rate when the a dipole moment is oriented parallel to the film plane. It is seen that the rate variation in the near zone (the region close to the film on both sides) is such that the relaxation process is dominated by emission into the interface mode channel. In the intermediate and far zones, the role of the interface modes is negligible and the dominant role is taken up by emission into the propagating and evanescent mode channels. At dipole positions far removed from the screen on either side, we recover the result $\Gamma_0(\varepsilon)$ appropriate for the unbounded dielectric in which the dipole is located.

3.2. Pair correlations

Consider a pair of identical dipole emitters, labelled 1 and 2, localised at the space points $\mathbf{r}_1$ and $\mathbf{r}_2$. The lowest excited state energy of the pair is $\hbar(\omega_e + \omega_g)$, corresponding to the state in which one of the emitters is in state $|e\rangle$ and the other in state $|g\rangle$. This quantum energy level is doubly degenerate and is spanned by two independent states, namely the symmetric state $|e_+\rangle$ and the antisymmeteric state $|e_-\rangle$ in the form $|e_\pm\rangle = \frac{1}{\sqrt{2}}\left(|e_1 g_2\rangle \pm |g_1 e_2\rangle\right)$. The ground state $|f\rangle = |g_1 g_2\rangle$ is singlet and has energy $2\hbar\omega_g$.

Both emitters interact with the same quantised field at their locations $\mathbf{r}_1$ and $\mathbf{r}_2$, so that the interaction Hamiltonian is $H_{int} = -\boldsymbol{\mu}_1.\mathbf{D}(\mathbf{r}_1, t)/\varepsilon_0 - \boldsymbol{\mu}_2.\mathbf{D}(\mathbf{r}_2, t)/\varepsilon_0$. The rates of de-excitation corresponding to the pair states $|e_\pm\rangle$ are functions of $\mathbf{r}_1$ and $\mathbf{r}_2$ and are given by

$$\Gamma^{\pm}(\mathbf{r}_1, \mathbf{r}_2) = \frac{2\pi}{\hbar^2} \sum_Q \left|\langle e_\pm, \{0\}\left|H_{int}\right| f, \{Q\}\rangle\right|^2 \delta(\omega_{if} - \omega_Q) \tag{4}$$

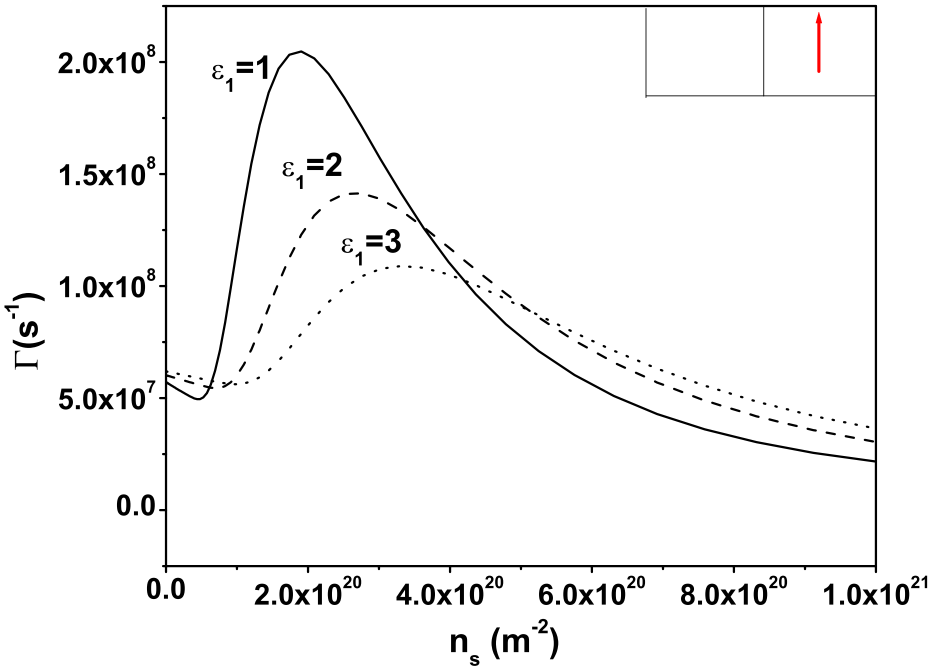

Figure 2: Variations of the dipole relaxation rate with the electron density n_s for a single dipole emitter of frequency ω_0 such that $\hbar\omega_0 = 2.0$ eV. The emitter is situated at a distance z = 50 nm in dielectric 2 (taken to be vacuum where $\varepsilon_2 = 1$) in front of the metallic sheet as an overlayer on three different types of dielectric 1, for which $\varepsilon_1 =$ 1, 2, and 3. See the text for a description of these results.

The transition frequency in both cases is $\omega_{if} = \omega_0 \equiv \omega_e - \omega_g$. The ensuing expressions can be written in the following form

$$\Gamma^{\pm}(\mathbf{r}_1, \mathbf{r}_2) = \frac{1}{2}\left\{\Gamma_0(\mathbf{r}_1) + \Gamma_0(\mathbf{r}_2)\right\} \pm \sum_{i,j} \hat{\mu}_i^{(1)} \hat{\mu}_j^{(2)} \Gamma_{ij}(\mathbf{r}_1, \mathbf{r}_2) \tag{5}$$

where $\Gamma_0(\mathbf{r}_1)$ and $\Gamma_0(\mathbf{r}_2)$ are the individual emission rates at the points where the dipole emitter 1 and dipole emitter 2 are localised, respectively. $\hat{\mu}_i^{(1)}$ and $\hat{\mu}_j^{(2)}$ are the ith and jth Cartesian vector components of unit vectors in the direction of the dipole moments of emitters 1 and 2, respectively. Γ_{ij} are functions of the the emitter positions. Unfortunately, even for the simplest cases, these analytical functions are too complicated to be displayed here. Meaningful results are obtainable with the help of numerical techniques. It is useful to select a few special cases for illustration purposes and, as we shall see, this is reasonably effective in uncovering interesting trends.

Figure 4 shows the variations of the ± emission rates for a pair of emitters with dipole vectors oriented parallel to the metallic film plane. Here dipole 1 is fixed at $z_1 = -20$ nm (near zone), while the position of dipole 2 varies across the sheet from left to right. The parameters are such that $\varepsilon_1 = 2.0; \varepsilon_2 = 1$ and metallic sheet density $n_s = 1.7 \times 10^{20}$ m^{-2}. The dipole oscillation frequency is such that $\hbar\omega_0 = 2.0$eV. There are three interesting observations here. First we note the strong enhancement in the near-zone, when dipole 2 is close to the surface on both sides of the screen. Secondly, when the position of dipole 2 coincides with that of dipole 1, on the left of the screen, we get the expected superradiance for Γ^+ and sub-radiance in Γ^-. However, identical behaviours can be seen when the position of dipole 2 is at the image position $z_2 \approx +20$nm, i.e. to the right of the screen. We deduce from this that there are superradiance and subradiance phenomena displayed by image-type

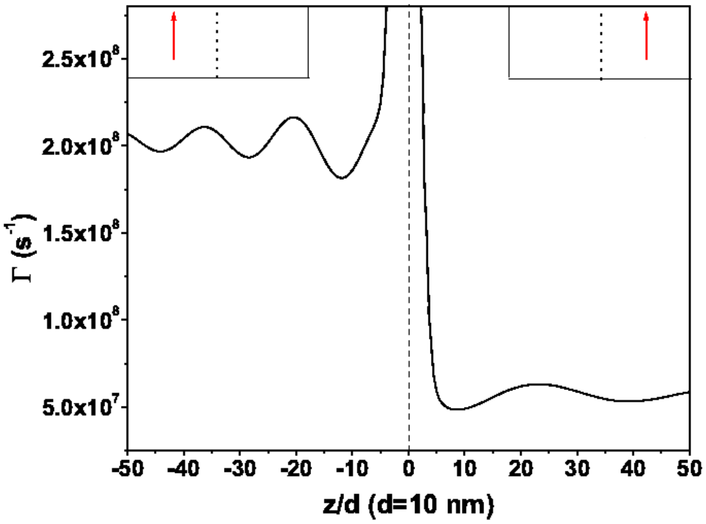

Figure 3: Variations of the emission rate with dipole position for a dipole of frequency ω_0 such that $\hbar\omega_0 = 2.0$ eV. The film electron density is $n_s = 51.73 \times 10^{20} m^{-2}$.

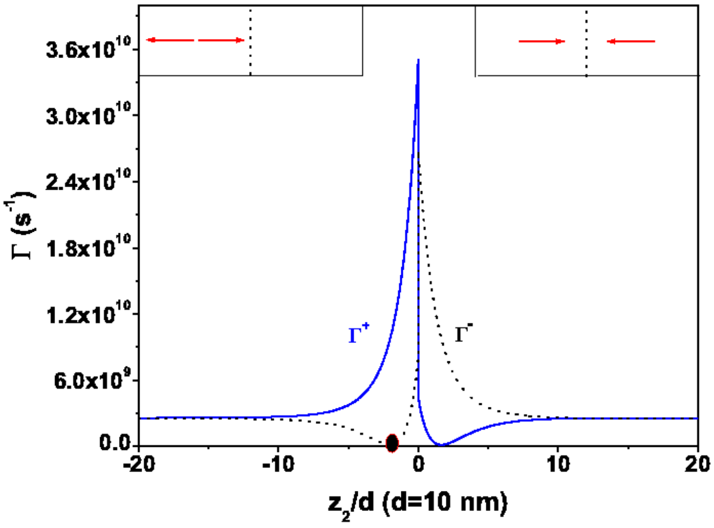

Figure 4: Cooperative rates $\Gamma^{\pm}$ in the near zone. Here dipole 1 is fixed at z_1 = -20 nm in region 1, where $\varepsilon_1 = 2$. Dipole 2 changes position from the left of the screen in region 1 to the right of the film in region 2, where $\varepsilon_2 = 1$. Here the dipoles are both antiparallel to interface as shown in the insets of the figure. The density of the film is $n_s = 1.7 \times 10^{20} m^{-2}$, and the value of the dipole frequency is $\hbar\omega_0 = 2$eV.

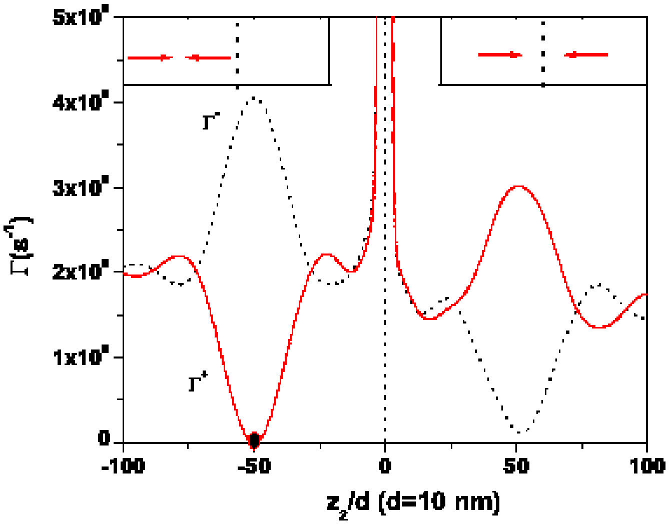

Figure 5: The cooperative rates $\Gamma^{\pm}$ in the far zone for the case $\varepsilon_2 = 1$ and $\varepsilon_1 = 4$. The two dipoles are both perpendicular to the film plane and antiparallel, with oscillation frequency ω_0 such that $\hbar\omega_0 = 2.0$ eV and the density is $n_s = 1.73 \times 10^{20} m^{-2}$. Dipole 1 is fixed at z_1= -500 nm and dipole 2 changes position across the screen.

effects. At the point $z_2 = 20$nm, dipole 2 and the image of dipole 1 coincide in position. The real dipoles are parallel, but at the image position, dipole 2 and the image of dipole 1 are antiparallel and we get superradiance for Γ^+ and subradiance for Γ^- at this position in this near-zone situation.

Figure 5 shows the situation in the far zone. Here dipole 1 is fixed at the position $z_1 = -500$nm and dipole 2 varies in position across the screen. When dipole 2 is far to the left or far to the right the dipole system displays oscillations with distance which are consistent with a dipole pair in free space. This interpretation can be confirmed by comparing a period of this oscillations with a transition wavelength $\lambda_0 = 2\pi/k_0$. In the right-hand region we see that superradiance and subradiance effects are exhibited by Γ^+ and Γ^-, respectively. However, on the left hand side, the situation is reversed: Γ^- shows superradiance and Γ^+ subradiance. This behaviour can be explained in terms of correlation between dipole 2 and the image of dipole 1 at $z = +500$nm. Note, however, that Γ^- is not exactly zero at $z_2 = +500$nm. This can be traced to the effects of a finite electron density. We have checked that as the density increases the superradiance behaviour $\Gamma^-(z_2) = +500$nm indeed vanishes, as it should.

4. QUANTUM EFFECTS NEAR MATERIAL WEDGES

Another dielectric cavity QED system is when dipole emitters are localised near the sharp end of a wedge-shaped dielectric slice of an arbitrary angle ϕ_0. The faces of the wedge are in contact with another material that, in general could be a dielectric or a metal, but here we shall consider the case of a wedge bordered by a high conductivity metal. As illustrated schematically in Fig. 6, the dipole emitter is situated in the wedge region at the general space point $\mathbf{R} = (\mathbf{r}_\parallel, 0) \equiv (r_\parallel, \phi, 0)$ in cylindrical polar coordinates, with the planar surfaces of the wedge defined by the equations $\phi = 0$ and $\phi = \phi_0$.

The evaluation of the de-excitation rate requires the construction of the displacement field vector operator $\mathbf{D}$ in terms of field quanta satisfying electromagnetic boundary conditions at the wedge interfaces. For perfectly conducting boundaries the field modes emerge as either transverse electric TE, for which $E_z = 0$ or transverse

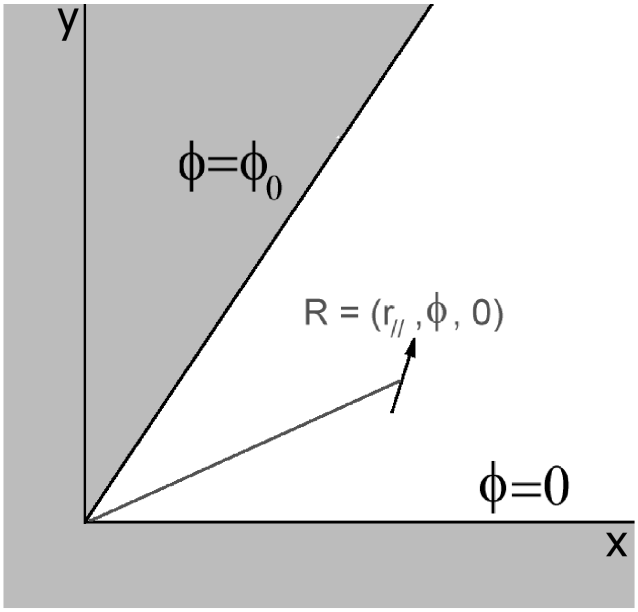

Figure 6: Schematic diagram representing the position of a dipole emitter of arbitrary orientation in a dielectric wedge, bounded by perfect conductor at $\phi = 0$ and $\phi = \phi_0$. The dipole emitter is represented by an arrow at the general cylindrical polar coordinate R = ($r_\parallel$, ϕ, z).

magnetic TM for which $B_z = 0$. Using cylindrical coordinates $\mathbf{R} = (\mathbf{r}_\parallel, z)$ we write

$$\mathbf{D}(\mathbf{R}) = \sum_{\eta=1,2} \sum_{n} \int d^2\mathbf{k}_\parallel \left\{ \boldsymbol{\mathcal{E}}^{(\eta)}_{\mathbf{k}_\parallel,n}(\mathbf{r}_\parallel, z, t) a_\eta(\mathbf{k}_\parallel, n) - h.c. \right\} \tag{6}$$

where $\mathbf{k}_\parallel$ is a two-dimensional wavevector in the $x-y$ plane. The operator $a_\eta(\mathbf{k}_\parallel, n)$ and its Hermitian conjugate are annihilation and creation operators for the quanta of the mode of polarisation η, where η is either TE for which $\eta = 1$, or TM, for which $\eta = 2$. The vector functions $\boldsymbol{\mathcal{E}}^{(\eta)}_{\mathbf{k}_\parallel,n}(\mathbf{r}_\parallel, z, t)$ are the mode spatial distribution functions. For TE modes, $\eta = 1$, the mode functions can be written as

$$\begin{aligned} \boldsymbol{\mathcal{E}}^{(1)}_{\mathbf{k}_\parallel,n}(\mathbf{r}_\parallel, z, t) &= \left(\frac{\hbar\omega}{2\pi\epsilon\phi_0 k_\parallel^2} \right)^{\frac{1}{2}} \left\{ J_m(k_\parallel r_\parallel) \frac{n\pi}{\phi_0} \sin\left(n\pi \frac{\phi}{\phi_0} \right) \frac{\hat{\mathbf{r}}_\parallel}{r_\parallel} \right. \\ &\quad - \left. \frac{\partial J_m(k_\parallel r_\parallel)}{\partial r_\parallel} \cos\left(n\pi \frac{\phi}{\phi_0} \right) \hat{\boldsymbol{\phi}} \right\} e^{i[k_z z - \omega(k_\parallel, n)t]} \end{aligned} \tag{7}$$

where carets denote unit vectors and k_z is given by $k_z^2 = \epsilon\omega/c^2 - k_\parallel^2$. In Eq.(7) and subsequently, $J_m(x)$ are Bessel functions, where m is related to integer $n \geq 0$ by $m = n\pi/\phi_0$. For the TM mode ($\eta = 2$) we have

$$\begin{aligned} \boldsymbol{\mathcal{E}}^{(2)}_{\mathbf{k}_\parallel,n}(\mathbf{r}_\parallel, z, t) &= \left\{ \xi(k_\parallel) \frac{\partial J_m(k_\parallel r_\parallel)}{\partial r_\parallel} \sin\left(n\pi \frac{\phi}{\phi_0} \right) \hat{\mathbf{r}} + \xi(k_\parallel) J_m(k_\parallel r_\parallel) \frac{n\pi}{\phi_0} \cos\left(n\pi \frac{\phi}{\phi_0} \right) \frac{\hat{\boldsymbol{\phi}}}{r_\parallel} \right. \\ &\quad + \left. k_\parallel J_m(k_\parallel r_\parallel) \sin\left(n\pi \frac{\phi}{\phi_0} \right) \hat{\mathbf{z}} \right\} \left(\frac{\hbar\omega}{2\pi\epsilon\phi_0 k_\parallel^2} \right)^{\frac{1}{2}} e^{i[k_z z - \omega(k_\parallel, n)t]} \end{aligned} \tag{8}$$

where $\xi(k_\parallel) = \left(1 - \frac{c^2 k_\parallel^2}{\epsilon\omega^2} \right)^{\frac{1}{2}}$. For obtuse angles, such as $3\pi/4$, the problem takes a totally new perspective; it becomes that of an emitter embedded in a bulk dielectric near and outside a metallic protrusion of wedge

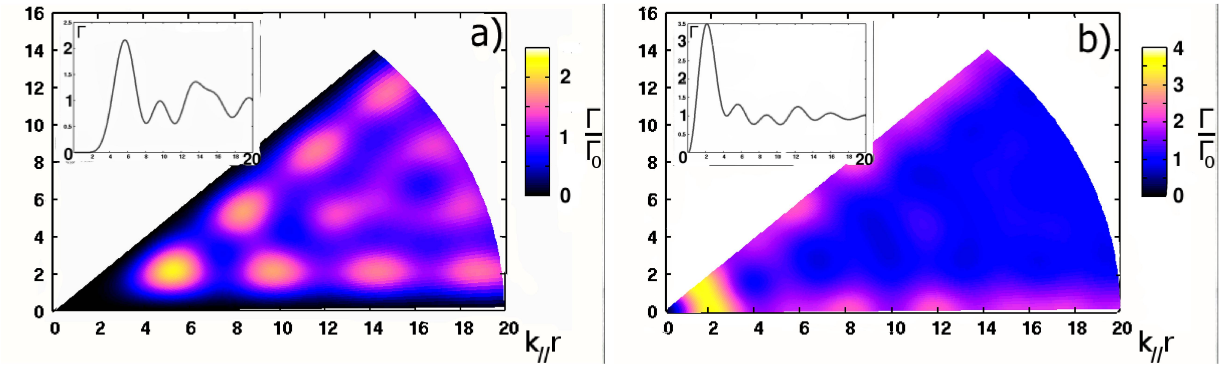

Figure 7: Dielectric wedge for which $\phi_0 = \pi/4$ embedded in a perfect conductor. The main figure shows the spatial distributions of the relative emission rate Γ/Γ_0 for dipole emitters in the x-y plane when the dipole moment is (a) oriented along the z axis (perpendicular case) and (b) oriented parallel to the x-y plane (along the azimuthal direction $\hat{\phi}$). Distances are in units of $1/k_0$ where $\lambda_0 = 2\pi/k_0$ is the dipole transition wavelength. The brightest regions represent maximum emission rates. The inset for each case shows the variation of the corresponding relative rate at points along the symmetry line $\phi = \pi/8$.

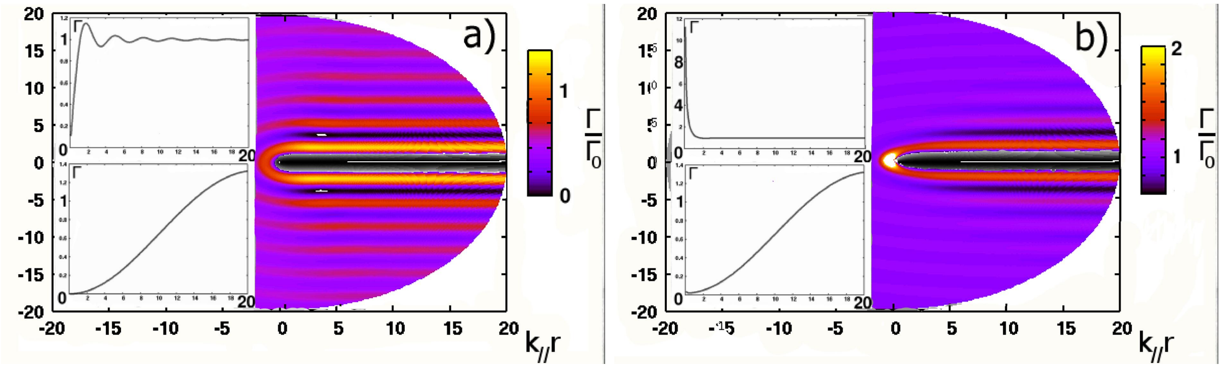

Figure 8: Metallic half-plane embedded in a dielectric $\phi_0 \approx 2\pi$. Spatial distributions of the relative emission rate,Γ/Γ_0, for dipole emitters in the x-y plane when the dipole moment is (a) oriented along the z axis (perpendicular case) and (b) oriented in the x-y plane (along the radial direction $\hat{r}_{\|}$). Distances are measured as in Fig. 7 and the brightest regions are regions of highest emission rates. The insets for each case show the variation of the corresponding relative rate at points along the symmetry line $\phi = \pi$ in the upper inset, and along a line at $\phi = \pi/50$ in the lower.

shape. In the limit of ϕ close to 2π we have an emitter localised near the edge of a metallic sheet. It should be emphasised that all elements of our formalism, including the quantised fields defined above, are applicable to all these cases with ϕ_0 assuming continuous values between 0 and 2π. It is possible to examine the manner in which the de-excitation rate distribution for emitters localised in the $z = 0$ plane evolves with changing angle ϕ_0 between the two extreme cases mentioned above. Illustrative results, as displayed in Figs. 7 and 8, are in the form of colour-coded graphs in which the rate is enhanced in certain regions (regions of superradiance) and suppressed in other regions (regions of sub-radiance).

In Figs. 7 and 8 we should note in particular the marked change in behaviour when the dipole orientation is switched from parallel (along the z-axis) and perpendicular (in the x-y plane). Note also that in the perpendicular polarisation case the region nearest to the wedge tip is a region of high suppression. Excited emitters situated in this region, in principle, preserve their state of excitation indefinitely. If an emitter situated in these dark regions is suddenly made to change its state of polarisation (for example by optical means) from perpendicular to parallel, the emitter should be de-excited and in certain positions the de-excitation process is enhanced. As we explain in the concluding section, we envisaged that this *in situ* control of de-excitation from subradiant to superradiant could be useful in quantum information processing.

We should also highlight the interesting extreme case of the system we have defined, namely the case in which the angle ϕ_0 becomes approximately equal to 2π. In this limit the dipole emitter is near a metallic half-plane occupying half the $x-z$ plane, with the rest of the space occupied by the dielectric. It is seen from Fig. 8 that the rate varies symmetrically round the line of termination (the z-axis) for all excited emitters localised in the dielectric in the vicinity of the edge. A change in the polarisation modifies the rate distribution near the edge markedly.

5. EMITTERS NEAR A 3D RIGHT ANGLE CORNER

Finally we consider a significant variant of the geometry involving material interfaces in which the main feature is a corner. For simplicity, we focus here on a case in which the physics is particularly transparent, namely a corner formed due to a right angle intersection of three planar conductor surfaces. The quantum systems are situated at fixed positions from the corner. The procedure for evaluating the emission rate can follow that for the edge case, but with the added complication that the fields in the vicinity of the corner have to satisfy the electromagnetic boundary conditions at three surfaces. In any case, the de-excitation rate for an emitter at $\mathbf{r}_0 = (x_0, y_0, z_0)$ emerges as the sum of eight terms

$$\Gamma = \Gamma_0 + \Gamma_{\mathbf{x}_0} + \Gamma_{\mathbf{y}_0} + \Gamma_{\mathbf{z}_0} + \Gamma_{\mathbf{x}_0\mathbf{z}_0} + \Gamma_{\mathbf{x}_0\mathbf{y}_0} + \Gamma_{\mathbf{y}_0\mathbf{z}_0} + \Gamma_{\mathbf{x}_0\mathbf{y}_0\mathbf{z}_0} \tag{9}$$

The first term is the de-excitation rate in an unbounded medium. The remaining terms arise from quantum interference due to the presence of the corner. We have

$$\Gamma_{\mathbf{u}_0} = \mathrm{Im}[\tilde{\mathbf{u}}\ \boldsymbol{\mu}\tilde{\Theta}(2\mathbf{u}_0)\boldsymbol{\mu}], \tag{10}$$

$$\Gamma_{\mathbf{u}_0\mathbf{v}_0} = \mathrm{Im}[\tilde{\mathbf{u}}\ \tilde{\mathbf{v}}\ \boldsymbol{\mu}^*\tilde{\Theta}(2\mathbf{u}_0 + 2\mathbf{v}_0)\boldsymbol{\mu}], \tag{11}$$

$$\Gamma_{\mathbf{x}_0\mathbf{y}_0\mathbf{z}_0} = \mathrm{Im}[\boldsymbol{\mu}^*\tilde{\Theta}(2\mathbf{x}_0 + 2\mathbf{y}_0 + 2\mathbf{z}_0)\boldsymbol{\mu}], \tag{12}$$

In the above $\mathbf{u}$ and $\mathbf{v}$ are $\mathbf{x}, \mathbf{y}$ or $\mathbf{z}$, such that $\tilde{\mathbf{u}}$ and $\tilde{\mathbf{v}}$ are reflection operators in the x, y, z planes, and $\mathbf{u}_0$ and $\mathbf{v}_0$ become $\mathbf{x}_0, \mathbf{y}_0$ or $\mathbf{z}_0$, where

$$\mathrm{Im}\left\{\boldsymbol{\mu_R}^*\tilde{\boldsymbol{\Theta}}(\mathbf{R})\boldsymbol{\mu}\right\} = \frac{3}{2}\Gamma_0\left\{\xi_1\frac{\sin\left(k_0R\right)}{k_0R} + \xi_3\left[\frac{\cos\left(k_0R\right)}{k_0^2R^2} - \frac{\sin\left(k_0R\right)}{k_0^3R^3}\right]\right\}, \tag{13}$$

is the imaginary part of the retarded dielectric tensor. The dipole orientation factors $\xi_p \equiv \xi_p\left(\mathbf{R}\right)$ are defined by

$$\xi_p = \hat{\boldsymbol{\mu}}_{\mathbf{R}}^*.\hat{\boldsymbol{\mu}} - p\left(\hat{\boldsymbol{\mu}}_{\mathbf{R}}^*.\hat{\mathbf{R}}\right)\left(\hat{\mathbf{R}}.\hat{\boldsymbol{\mu}}\right); \qquad (p = 1, 3) \tag{14}$$

where carets denote unit vectors and $\boldsymbol{\mu}_{\mathbf{2x_0}} = \tilde{\mathbf{x}}\boldsymbol{\mu}$; $\boldsymbol{\mu}_{\mathbf{2y_0}} = \tilde{\mathbf{y}}\boldsymbol{\mu}$ and $\boldsymbol{\mu}_{\mathbf{2x_0+2y_0}} = \tilde{\mathbf{x}}\tilde{\mathbf{y}}\boldsymbol{\mu}$. The notation is such that, for instance, $\tilde{\mathbf{x}}\mathbf{r}_0 \equiv (x_0, -y_0, 0)$, $\tilde{\mathbf{y}}\mathbf{r}_0 \equiv (-x_0, y_0, 0)$, and $\tilde{\mathbf{x}}\tilde{\mathbf{y}}\mathbf{r}_0 \equiv (-x_0, -y_0, 0)$.

Figure 9 shows the spatial distribution of the emission rate when the dipole moment vector of the emitter is directed along the z-axis. This figure is in the form of a set of colour-coded contour plots presenting the variation of Γ/Γ_0 at emitter positions (x_0, y_0, z_0) where z_0 is the value of z defining the plane. The planes are separated by distance $\lambda/4\pi$, where λ is the dipole transition wavelength. Within a given plane $z = z_0$ the rate is seen to be subradiant near the $x = 0$ and $y = 0$ planes and there are clear regions of superradiance, as in the edge case.

6. CONCLUSIONS

In conclusion, we have systematised a procedure for modelling quantum optical processes and pair correlation effects for radiating dipolar quantum systems localised at well defined distances of the order of a dipole transition wavelength from dielectric cavity surfaces. The cavity structures we have concentrated on are in the form of planar asymmetric metallic film sandwiteched between two dielectrics, dielectric wedges and corners in contact

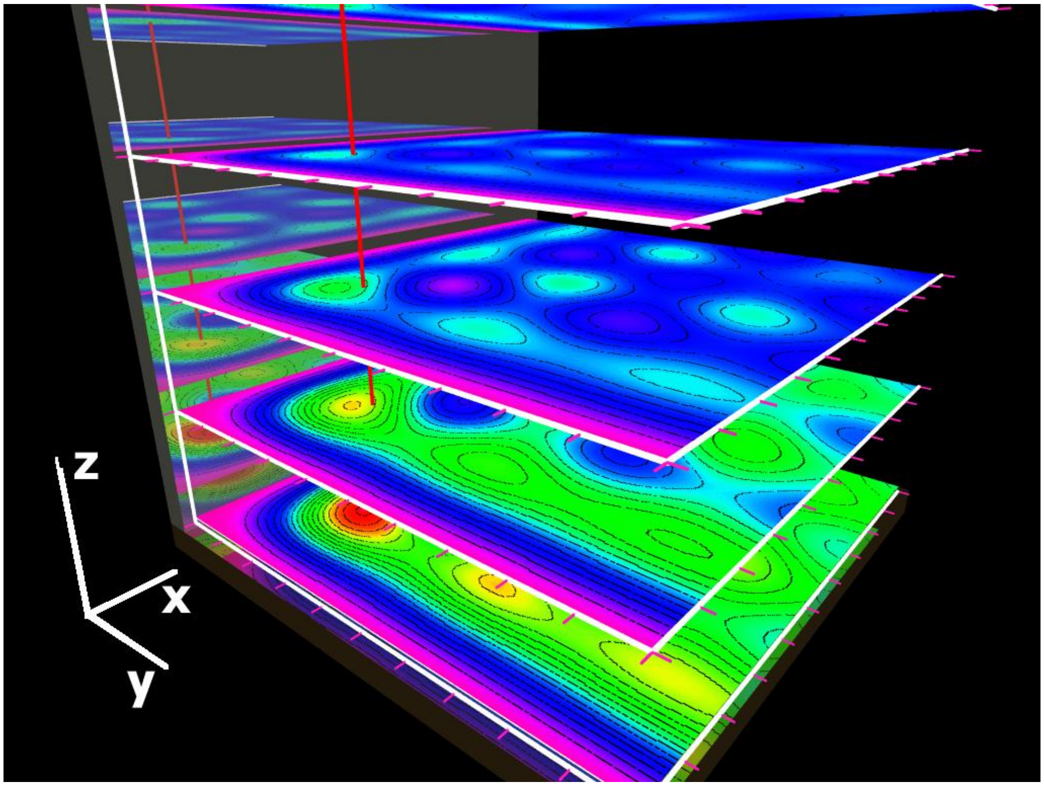

Figure 9: Colour-coded spatial distributions of the relative emission rate Γ/Γ_0 when the emitter dipole moment vector is parallel to the z-axis, $\boldsymbol{\mu} = (0,0,\mu)$. This figure consists of a set of contour plots, each plot showing the variation of the relative emission rate on a plane defined by a certain value of z_0=0,$\lambda/4\pi$,$\lambda/2\pi$,$3\lambda/4\pi$. The red regions represent the highest values, and the purple regions lowest values of the relative emission rate. The tick marks on the plane edges are spaced at units of $\lambda/2\pi$.

with a high conductivity metal, but these are primarily for illustration purposes; any desired shape and material combinations forming the electromageneic environment can, in principle, be dealt with in a similar manner. The key common observation is that there are distinct regions where the emitter is subject to suppression and enhancement of the de-excitation process, depending on the dipole orientation. The details of our predictions should be verifiable experimentally for transitions in the optical region of the spectrum. However, a proof of principle, experiment has been conducted in the RF region of the spectrum using a radiowave antenna as the dipolar emitter situated between conductor planes at an angle, forming a wedge.[12] This set-up follows the work by Seeley et al[13] for a parallel planes. The results of the experiment are in excellent agreement with the theoretical predictions shown here for the wedge case. However, the details of this and extended experimental work will not be discussed any further here.

We suggest that this scenario could be exploited as a basis for the design of a scalable architecture for quantum information processing. This suggestion became more persuasive following the success of experiments which, for the first time, were able to demonstrate quantum cryptography using a nitrogen vacancy in a diamond nanocrystal as a single-photon source[14].[15] Suitable emitters, such as atoms, molecules, or quantum dots, could be positioned at well defined locations and their dipole moment vectors can be optically controlled. Our results suggest that emission could be switched on and off, simply by a change of the dipole orientation. Furthermore, we have seen that the emission process can be viewed as a coopertaive effect between the dipole and its set of images in the conductors. In fact it is easy to see that in the present situation, the emission process arises as a transition from a definite entangled symmetric excited state of the emitter and its images. For two identical emitters near an edge, the expected two-body entanglment should be modified significantly by the quantum interference. The possibility of the applicability of the work presented here to the area of quantum information processes rests in the suggestion that the de-exciation rate of dipole emitters can be controlled optically from totally dark to superradiant by a change of dipole orientation. The dielectric environment should be particularly helpful for emitters in the form of a colour centre, since in that case any recoil on emission is carried away by the whole crystal, removing one of the sources of unwanted decoherence. Work is now in progress to expolre the two-body and multi-body cooperative effects in the same environment since such effects are envisaged to be important for the realisation of quantum gates[16][17].[18] It would be intereting also to find out how transfer of energy between such emitters is influenced by their proximity to the narrow end of such material wedges. The experimental realisation of such a system should not pose great difficulties since any desired shape can now be created, thanks to recent advances in material preparation at the nanoscale using modern deposition techniques and lithography. These advances, coupled with parallel advances in the detection of atomic and molecular position to nanometer accuracy[3] should make the predictions we have made here amenable to experimental investigation. The two-body entanglement need not be for emitters on the same $x - y$ plane, but the emitters could be on different planes near the edge and their dipole moment vectors could be oriented in arbitrary directions. Work on this relatively more complicated situation is now in progress.

REFERENCES

1. E. A. Hinds, *Adv. At. Mol. Opt. Phys.* **28**, pp. 237 (1991)
2. C. Welch and J. Burgoyne,*Physics World; Vacuum Challenges and Solutions*, volume 19, pp. 21 (2006)
3. J. Michaelis, C. Hettish, M. Mlynek and V. Sandoghdar, *Nature* **405**, pp. 325 (2000)
4. M. Babiker, *J. Phys.: Condens Matter* **5**, pp. 2137 (1993)
5. M. Al-Amri and M. Babiker, *Phys. Rev. A* **67**, pp. 043820 (2003)
6. M. Al-Amri and M. Babiker, *Phys. Rev. A* **69**, pp. 065801 (2004)
7. S. Al-Awfi and M. Babiker, *Phys. Rev. A* **61**, pp. 033401 (2000)
8. S. Al-Awfi and M. Babiker, *Phys. Rev. A* **58**, pp. 4768-4778 (1998)
9. G. Banyard, C. R. Bennett and M. Babiker, *Opt. Commun.* **207**, pp. 195 (2002)
10. C. R. Bennett, J. B. Kirk and M. Babiker, *Phys. Rev. A* **63**, pp. 033405 (2001)
11. M. A. Kaliteevski, S. Brand, R. A. Abram, V. V. Nikolaev, M. V. Maximov, C. M. Sotomayor Torres, C M and A. V. Kavokin, *Phys. Rev. B***64** 115305 (2001)
12. Tal Marciano, H. Toubiana, M. Jacka, S. C. Skipsey and M. Babiker, *"Study of Dipole radiation between mirrors with variable geometry" (Unpublished).*
13. F. B. Seeley, J. E. Alexander, R. W. Connaster, J. S. Conway and J. P. Dowling, *Am. J. Phys.* **61**, pp. 545 (1993)
14. A. Beveratos, R. Brouri, T. Cacoin, J. P. Poizat and P. Grangier, *Phys. Rev. A* **64**, pp. 061802(R) (2001)
15. A. Beveratos, R. Brouri, J. P. Poizat and P. Grangier, *Opt. Lett.* **25**, pp. 1294 (2000)
16. D. Jaksch, J. I. Cirac, P. Zoller, S. R. Rolston, R. Cote and M. D. Lukin, *Phys. Rev. Lett.* **85**, pp. 2208 (2000)
17. T. Calcaco, A. Datta., P. Fedichev, E. Pazy and P. Zoller, *Phys. Rev. A* **68**, pp. 012310 (2003)
18. U. Dorner, P. Fedichev, D. Jaksch, M. Lewinstein and P. Zoller, *Phys. Rev. Lett.* **91** pp. 073601 (2003)